The EMBO Journal (2006) 25, 1375–1384 | © 2006 European Molecular Biology Organization | All Rights Reserved 0261-4189/06
www.embojournal.org

THE EMBO JOURNAL

Structure of glutamate carboxypeptidase II, a drug target in neuronal damage and prostate cancer

Jeroen R Mesters[1,4], Cyril Barinka[2,4,5], Weixing Li[3], Takashi Tsukamoto[3], Pavel Majer[3], Barbara S Slusher[3], Jan Konvalinka[2] and Rolf Hilgenfeld[1,*]

[1]Institute of Biochemistry, Center for Structural and Cell Biology in Medicine, University of Lübeck, Lübeck, Germany, [2]Institute of Organic Chemistry and Biochemistry, Academy of Science of the Czech Republic, Prague, Czech Republic and [3]Guilford Pharmaceuticals Inc., Baltimore, MD, USA

Membrane-bound glutamate carboxypeptidase II (GCPII) is a zinc metalloenzyme that catalyzes the hydrolysis of the neurotransmitter *N*-acetyl-L-aspartyl-L-glutamate (NAAG) to *N*-acetyl-L-aspartate and L-glutamate (which is itself a neurotransmitter). Potent and selective GCPII inhibitors have been shown to decrease brain glutamate and provide neuroprotection in preclinical models of stroke, amyotrophic lateral sclerosis, and neuropathic pain. Here, we report crystal structures of the extracellular part of GCPII in complex with both potent and weak inhibitors and with glutamate, the product of the enzyme's hydrolysis reaction, at 2.0, 2.4, and 2.2 Å resolution, respectively. GCPII folds into three domains: protease-like, apical, and C-terminal. All three participate in substrate binding, with two of them directly involved in C-terminal glutamate recognition. One of the carbohydrate moieties of the enzyme is essential for homodimer formation of GCPII. The three-dimensional structures presented here reveal an induced-fit substrate-binding mode of this key enzyme and provide essential information for the design of GCPII inhibitors useful in the treatment of neuronal diseases and prostate cancer.

The EMBO Journal (2006) **25,** 1375–1384. doi:10.1038/sj.emboj.7600969; Published online 9 February 2006
Subject Categories: neuroscience; structural biology
Keywords: NAALADase; neurodegenerative disease; peptidase; prostate cancer; PSMA

Introduction

Excessive activation of ionotropic glutamate receptors has been implicated in acute as well as chronic neurodegenerative disorders including stroke (Benveniste *et al*, 1984; Fagg *et al*, 1986; Butcher *et al*, 1990) and amyotrophic lateral sclerosis (ALS; Shaw and Ince, 1997). Conventional therapies have focused on blockade of postsynaptic glutamate receptors with small molecules. *N*-methyl-D-aspartate (NMDA) receptors have received the most attention culminating in several antagonists, which, however, tend to negatively affect learning and memory (Doble, 1999).

An alternative to the blocking of glutamate receptors is to reduce the levels of presynaptic glutamate. One important source of presynaptic glutamate is *N*-acetyl-L-aspartyl-L-glutamate (NAAG; Figure 1A). This neurotransmitter is found in millimolar concentrations in the brain (Coyle, 1997), where it can undergo hydrolysis to *N*-acetyl-L-aspartate (NAA) and L-glutamate. Synaptic hydrolysis of NAAG is catalyzed by glutamate carboxypeptidase II (GCPII, E.C. 3.4.17.21), a membrane-bound enzyme initially known as NAALADase (*N*-acetylated α-linked acidic dipeptidase; Robinson *et al*, 1987; Slusher *et al*, 1990; Berger *et al*, 1995; Carter *et al*, 1996). Interfering with glutamate production through GCPII inhibition has been substantiated as a promising approach for the treatment of stroke (Slusher *et al*, 1999), ALS (Ghadge *et al*, 2003), chronic pain (Yamamoto *et al*, 2001a, b; Chen *et al*, 2002; Carpenter *et al*, 2003; Majer *et al*, 2003; Kozikowski *et al*, 2004), diabetic neuropathy (Zhang *et al*, 2002), and other neurological disorders associated with glutamate excitotoxicity (Jackson and Slusher, 2001). GCPII inhibition results in increased NAAG levels and reduced glutamate levels. NAAG has been shown to be a partial NMDA receptor antagonist (Sekiguchi *et al*, 1989; Puttfarcken *et al*, 1993) as well as an agonist for the metabotropic (i.e., G-protein-coupled) glutamate receptor-3 (mGluR3, Wroblewska *et al*, 1997). As NMDA antagonists (Rogawski, 1993) and mGluR3 agonists (Bruno *et al*, 1995) have been found to be neuroprotective, GCPII inhibition can provide neuroprotection by both elevation of NAAG and reduction of glutamate levels. Hydrolysis of NAAG also occurs upon electrical hyperstimulation through increased GCPII activity (Urazaev *et al*, 2001), suggesting that GCPII is overactivated in pathological states.

GCPII is identical to prostate-specific membrane antigen (PSMA; Carter *et al*, 1996; Tiffany *et al*, 1999), a tumor marker in prostate cancer (Su *et al*, 1995). GCPII is also found in the membrane brush border of the small intestine where it acts as a folate hydrolase (Pinto *et al*, 1996; Heston, 1997). This reaction expedites intestinal uptake of folate through hydrolysis of folylpoly-γ-glutamates (Figure 1B; Tasch *et al*, 2001; Ghosh and Heston, 2004). Conceivably, GCPII inhibitors could be helpful in the imaging and treatment of tumors where folate is required for their growth.

GCPII is a 750-residue, membrane-associated dinuclear zinc peptidase (MEROPS clan MH, subfamily M28B; Rawlings *et al*, 2004) of a total molecular weight of 110 kDa, including *N*-glycosylation in no less than 10 sites in the full-length protein (Holmes *et al*, 1996; Ghosh and Heston, 2003; Barinka *et al*, 2004). Being a class II membrane protein, GCPII has a short cytosolic amino-terminal region of approximately 19 residues and a single membrane-spanning segment (about 22 residues), with the bulk of the protein being located in the extracellular space.

*Corresponding author. Institute of Biochemistry, Center for Structural and Cell Biology in Medicine (CSCM), University of Lübeck, Ratzeburger Allee 160, D-23538 Lübeck, Germany.
Tel.: +49 451 500 4060; Fax: +49 451 500 4068;
E-mail: hilgenfeld@biochem.uni-luebeck.de
[4]These authors contributed equally to this work
[5]Present address: Center for Cancer Research, National Cancer Institute, Frederick, MD 21702, USA

Received: 1 September 2005; accepted: 23 December 2005; published online: 9 February 2006

©2006 European Molecular Biology Organization

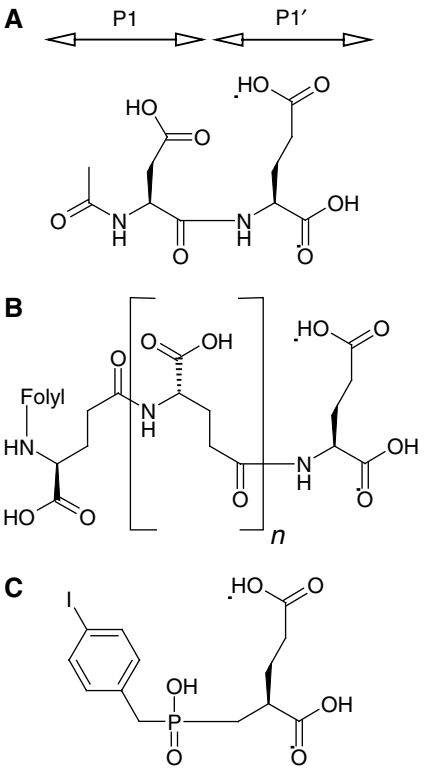

Figure 1 Chemical formulae for (**A**) *N*-acetyl-L-aspartyl-L-glutamate (NAAG), (**B**) folyl-poly-γ-glutamate, (**C**) (*S*)-2-(4-iodobenzylphosphonomethyl)-pentanedioic acid (GPI-18431). The P1 and P1′ moieties are indicated for (A).

Several derivatives of 2-(phosphonomethyl)-pentanedioic acid (2-PMPA) have been described as selective inhibitors of GCPII, with the best of them exhibiting IC_{50} values in the range of 0.3–30 nM (Slusher *et al*, 1999; Jackson *et al*, 2001). Here we report the crystal structure of the fully glycosylated extracellular domains (residues 44–750) of GCPII in complex with the 2-PMPA derivative, (*S*)-2-(4-iodobenzylphosphonomethyl)-pentanedioic acid (GPI-18431, $IC_{50} = 30$ nM; Tsukamoto *et al*, 2005; Figure 1C) at 2.0 Å resolution. In addition, we describe the crystal structure of the enzyme with a phosphate ion bound to the catalytic center, at 2.4 Å resolution. Phosphate is a weak inhibitor of the recombinant GCPII, with an IC_{50} of 10 μM (Barinka *et al*, 2002). Finally, we report the structure of a complex with the product of the catalytic reaction, glutamate, at 2.2 Å resolution.

The three crystal structures correspond to different states of the active site and reveal an induced-fit mechanism for the enzyme. They provide the basis for the design of better inhibitors of GCPII, especially in view of the fact that the published theoretical model for the enzyme–substrate interactions (Rong *et al*, 2002) is not correct. Unfortunately, this is also true for a model derived from a very-low-resolution (3.5 Å) crystal structure of PSMA that was described recently (Davis *et al*, 2005).

Results

Overall structure

The 2.0-Å resolution structure of the extracellular portion of GCPII (residues 44–750) in complex with GPI-18431 (Figure 1C), an iodobenzyl derivative of the potent inhibitor 2-PMPA, was determined by single-wavelength anomalous dispersion (SAD), making use of the zinc ions at the catalytic center of the enzyme, along with a strong contribution from the iodine atom present in the inhibitor (see Supplementary Table 1). Crystals of the GCPII complexes with phosphate and glutamate were isomorphous to the complex with GPI-18431. The structures were determined by difference Fourier methods and refined to 2.4 and 2.2 Å resolution, respectively (Supplementary Table 1). The overall root-mean-square deviations (r.m.s.d.) of the backbone atoms between the GPI-18431 complex structure on the one hand and the phosphate and glutamate complexes on the other are 0.27 Å for 657 Cα pairs (out of 677 compared) and 0.21 Å for 665 Cα pairs (out of 682), respectively.

The extracellular portion of GCPII folds into three distinct domains: the protease domain (domain I, residues 57–116 and 352–590), the apical domain (domain II, residues 117–351), and the C-terminal domain (residues 591–750) (Figure 2). Amino-acid residues from all three domains are involved in substrate recognition. Although the asymmetric unit of the crystal contains a monomer of GCPII, a homodimer is formed through crystallographic two-fold symmetry. A dimer was also reported to be the active species of GCPII in solution (Schulke *et al*, 2003).

The fold of the protease domain I is most closely related to the aminopeptidases of *Aeromonas proteolytica* (PDB code 1AMP, Chevrier *et al* (1994); r.m.s.d. 2.0 Å for 239 Cα pairs out of 291 compared) and *Streptomyces griseus* (1XJO, Greenblatt *et al* (1997); r.m.s.d. 2.1 Å for 243 Cα pairs out of 277). The dominant structural feature of this domain is a central seven-stranded mixed β-sheet with 10 flanking α-helices. Strand β1 and its antiparallel mate β9, which are the first and second strands of the central β-sheet of the protease domain, connect domains I and II.

Inserted between the first and second strand of the central β-sheet of the protease domain is the apical domain (domain II) that covers the active site, creating a deep substrate-binding funnel between the domains. The central (3 + 4)-stranded β-sandwich of the apical domain is flanked by four α-helices. The domain harbors four solvent-exposed, consecutive proline residues (Pro146–149) following strand β3 that make up a perfect polyproline type-2 helix.

The main feature of the C-terminal domain (domain III) is an Up–Down–Up–Down four-helix bundle formed by helices α15, α17, α18-α19, and α20. The loop following α15 contains the two-turn helix α16, which is oriented almost perpendicular to the helix bundle. Helix α18 is followed by two loops, the first of which (residues 676–690) reaches out to contact domain I through hydrogen bonds (see Supplementary Table 2). At the C-terminal end of this first loop, the polypeptide chain returns to complete helix α18, with the amide nitrogen of Val690 forming its C-cap. This unusual feature is followed by the second loop, the β-hairpin β15/β16 (residues 692–704; colored green in Figure 2), which is also involved in several hydrogen bonds to domain I (Supplementary Table 2). Being part of the hairpin (the 'glutarate sensor'), residues Lys699 and Tyr700 are directly involved in the specific binding of the glutarate (pentanedioic acid) portion of GPI-18431 and of glutamate (see below). Beyond the two loops, the polypeptide chain returns into the bundle to form α19, which can be seen as a continuation of α18.

 ©2006 European Molecular Biology Organization

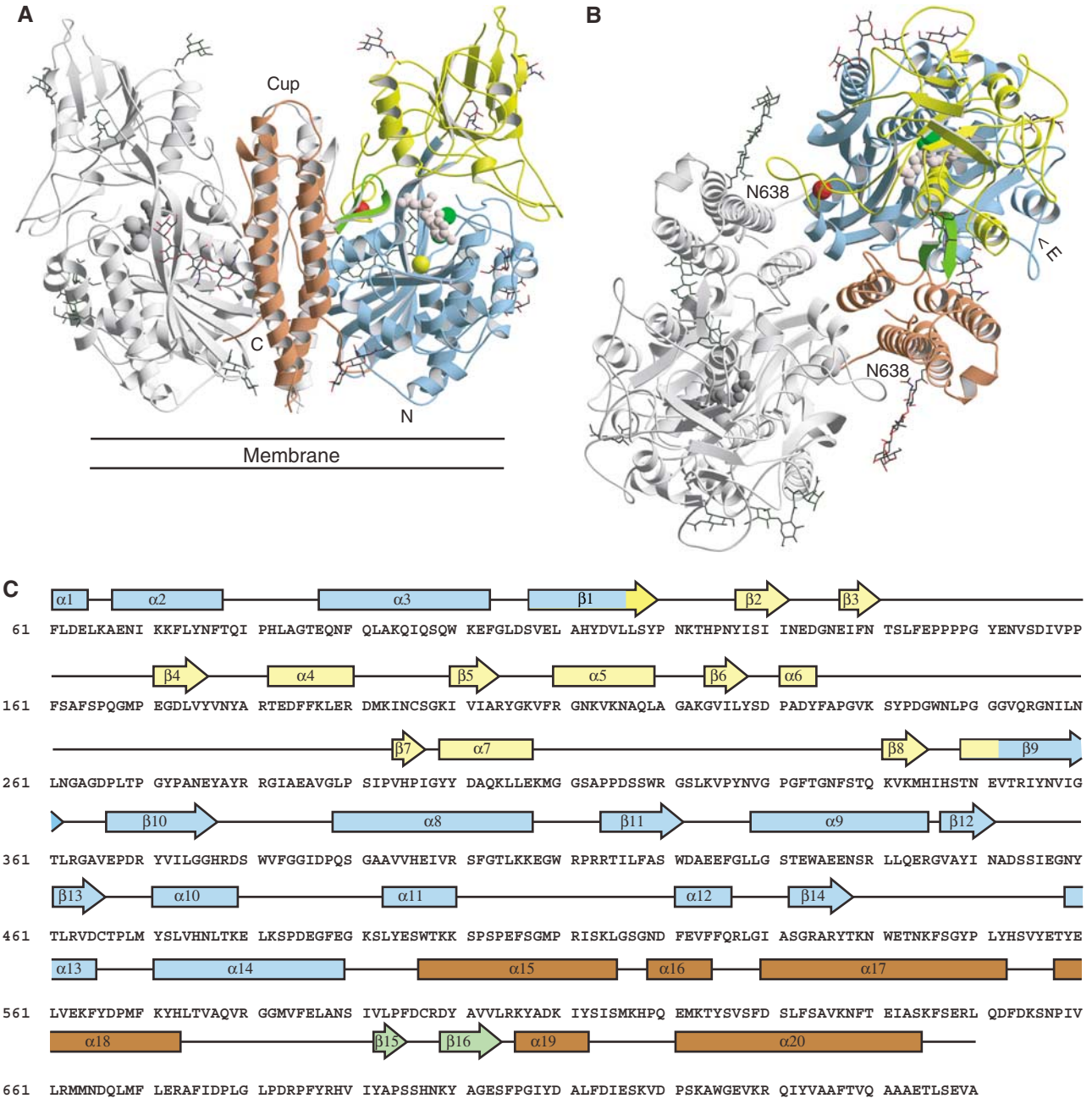

Figure 2 Structure of GCPII. (**A, B**) Three-dimensional structure of the dimer. One subunit is shown in gray, while the other is colored according to organization into domains. Domain I, light blue; domain II, yellow; domain III, brown. The dinuclear zinc cluster at the active site is indicated by dark green spheres, the Ca^{2+} ion near the monomer–monomer interface by a red sphere, and the Cl^{-} ion by a yellow sphere. The GPI-18431 inhibitor is shown as small beige balls. The 'glutarate sensor' (the β15/β16 hairpin) is shown in light green. The seven carbohydrate side chains located in the electron density maps are indicated. The position of the structure relative to the membrane is shown in (A). (B) Provides a view into the 'cup' of the dimeric enzyme (see text). The entrance to the catalytic site is indicated ('E'). (**C**) Primary and secondary structure of GCPII, colored according to domain organization. Domain I, light blue; domain II, yellow; domain III, brown.

Dimer formation

The C_2-symmetric homodimer features a dimerization interface of about 2457 Å^2, mostly comprised of domain III of one monomer and domains I and II of the other (Figure 2A and B, Supplementary Table 2). In addition, there are two intermolecular domain III—domain III salt-bridges formed across the two-fold axis between Arg662 Nη1 of helix α18 of one monomer and Asp666 Oδ2 of the same helix of the other monomer.

We located one calcium ion in the GCPII structure. It is coordinated by domain I residues Glu433 (both Oε1 and Oε2) and Glu436 (Oε2), as well as by domain II residues Thr269 (Oγ1 and main-chain O) and Tyr272 (main-chain O), at distances between 2.31 and 2.51 Å. The seven-fold coordination is completed by a water molecule (2.44 Å). The Ca^{2+} is too remote (>19 Å) from the active site to be involved in the catalytic activity. More likely, its role is to hold domains I and II together through coordinative interactions. Furthermore, it is probably important for dimerization by stabilizing the loop 272–279, which carries three tyrosine residues (272, 277, 279) that form a hydrophobic pocket. This site is entered by the side chain of Tyr733 (helix α20) of the other monomer in

©2006 European Molecular Biology Organization

the dimer. In addition, Tyr277 makes an intermolecular hydrophobic interaction with the *N*-acetyl group of NAG_I of the sugar chain attached to Asn638 (see below).

Glycosylation sites

Seven out of 10 possible *N*-glycosylation sites (N-X-S/T motif) present in the recombinant ectodomain carry carbohydrates that are visible in the electron density. For most of these, we were able to locate one or two *N*-acetylglucosamine (NAG) residues in difference maps. In contrast, the sugar residues at Asn638 of helix α17 (brown in Figure 2B) were much better defined in the maps: Two NAG and two mannose units were visible in the electron density, with the sugars clearly contributing to dimer formation by making contacts to domain II ($638NAG_{II}$ O4…Glu276 Oε2, 3.38 Å, $638Man_I$ O2…Glu276 Oε2, 2.02 Å) and to strands β1 and β9 at the domain I–II interface ($638Man_{II}$ O3…Arg354 Nη1, 3.46 Å; $638Man_I$ O2…Arg354 Nη1, 3.25 Å). This interaction is one of the few structurally well-defined cases of a protein–carbohydrate contact involved in homodimerization of a protein.

Active site

A ~20 Å deep funnel leads from the surface of GCPII to the active site that contains two zinc ions (Figure 3). Each of these is ligated to one oxygen of the phosph(in)ate moiety in the GPI-18431 and phosphate complexes (Figure 4A and B). Zn…O(phosph(in)ate) distances are between 1.75 and 1.93 Å. In the glutamate complex (Figure 4C), the catalytic zinc center is in its free state, and a single water molecule (or hydroxide anion) bridges the two metal ions, in an asymmetric fashion (H_2O…Zn(1), 1.79 Å; H_2O…Zn(2), 2.26 Å). Interestingly, the distance between the two zinc ions varies considerably, from 3.30 Å in the free state (i.e., in the glutamate complex) to 3.65 and 3.78 Å, respectively, in the complexes with phosphate and GPI-18431. In addition, the two metal ions are bridged by Asp387 (1.95–2.03 Å to Zn(1); 1.76–1.90 Å to Zn(2); distance range observed in the different structures). Notably, the Asp387-Pro388 peptide bond is in the *cis* conformation in all three structures (this is common in dinuclear zinc peptidases). Additional ligands for Zn(1) are His377 (1.94–2.01 Å) and Asp453 (1.94–2.07 Å), and for Zn(2), Glu425 (1.81–1.97 Å) and His553 (2.04–2.16 Å). Thus, each of the two zinc ions is tetrahedrally coordinated, although with a distance of 2.39–2.49 Å between its second carboxylate oxygen and Zn(2), Glu425 could also be considered a bidental ligand, and Zn(2) 5-fold coordinated. The phosph(in)ate oxygen interacting with Zn(2) also accepts a hydrogen bond (2.80, 2.86 Å; here and in the rest of this paragraph, the first number refers to the complex with GPI-18431 and the second to the one with phosphate) from the phenolic OH group of Tyr552 (Figure 4A and B). One of the two phosphate oxygens not interacting with the zinc ions makes hydrogen-bonding interactions with Glu424 (3.04, 2.77 Å) and Tyr552 (2.80, 2.86 Å). In spite of the significant difference in the Zn…Zn distance between the ligated and free states of the catalytic center, none of the distances between the metal ions and their ligands changes by more than 0.15 Å.

Catalytic mechanism

Glu424 is the likely catalytic acid/base of GCPII (Speno *et al*, 1999). In the glutamate complex, that is, in the free state of the catalytic center, one of its carboxylate oxygens is hydrogen-bonded (2.56 Å) to the water molecule bridging the two zinc ions, whereas the other interacts (2.68 Å) with the free amino group of the bound glutamate, the product of the cleavage reaction. This is in agreement with the function of Glu424 as a proton shuttle that abstracts a proton from the zinc-bound catalytic water and, during or after substrate cleavage, transfers it to the leaving group, the amino moiety of glutamate (Figure 5). Activated through the initial proton abstraction, the catalytic water will attack the carbonyl group

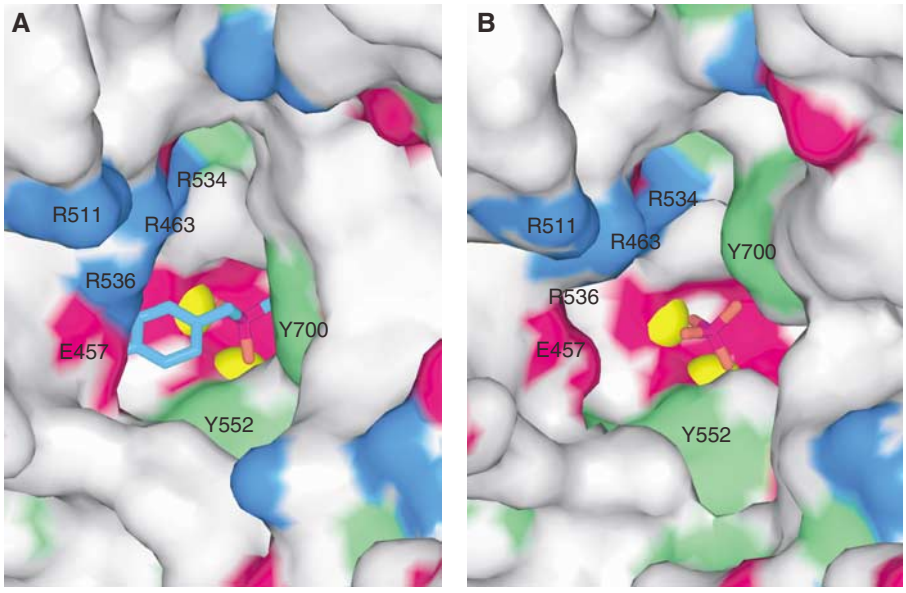

Figure 3 Surface representation of the ~20 Å deep funnel leading to the catalytic site. Blue, side-chain nitrogens of Arg and Lys residues; red, side-chain oxygens of Asp and Glu; green, side-chain carbons of Tyr and Phe residues. Yellow, Zn^{2+} ions; inhibitors shown as stick models. (**A**) Complex with GPI-18431; (**B**) complex with phosphate. Note the difference in the shape of the pocket because of withdrawal of the 'glutarate sensor' (Y700) in the phosphate complex.

 ©2006 European Molecular Biology Organization

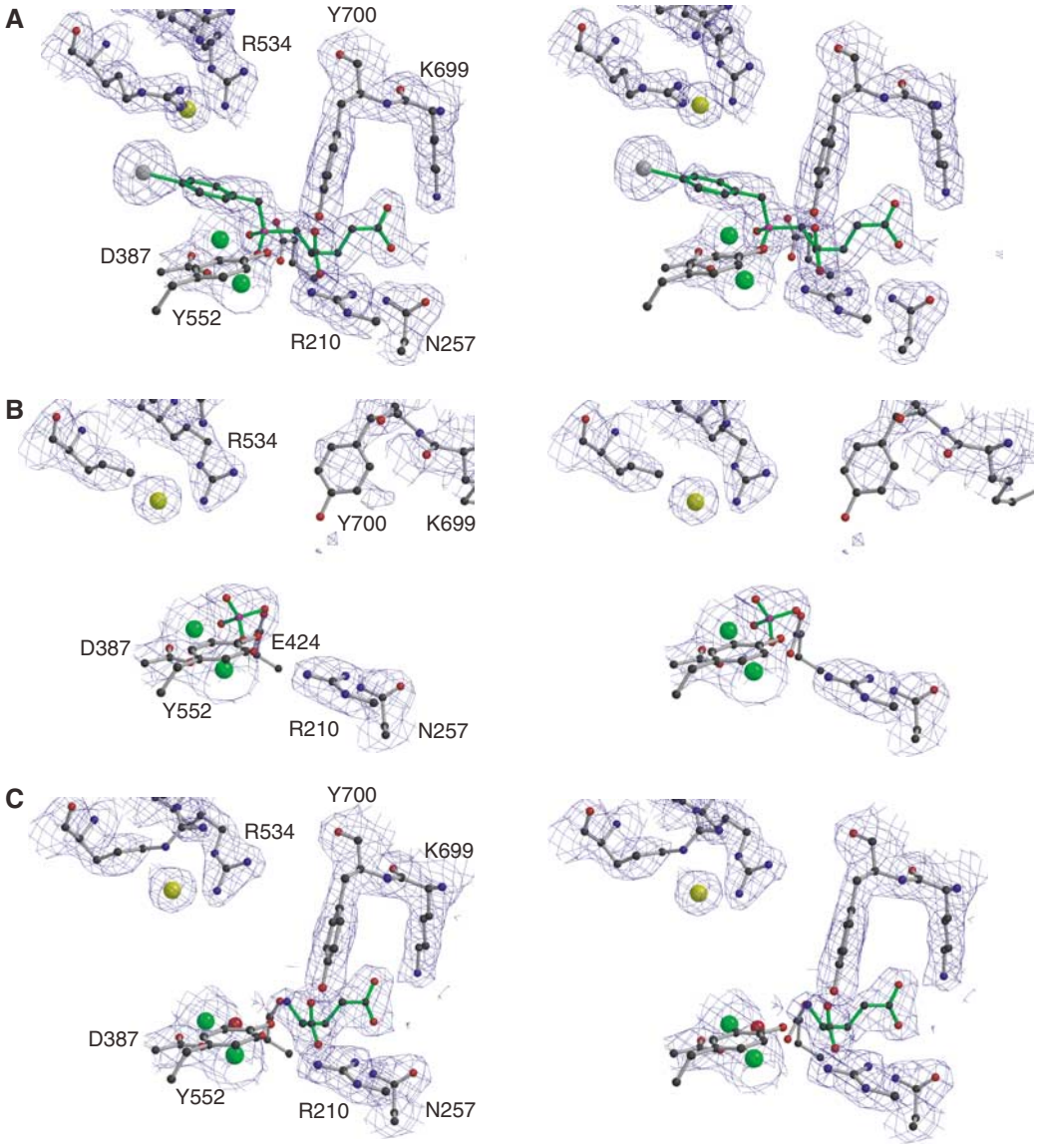

Figure 4 $2F_o$–F_c electron density maps (stereo) contoured at 1.2σ, for the GCPII complex with GPI-18431 (**A**), phosphate (**B**), and L-glutamate (**C**). Zinc ions are shown in dark green, chloride in yellow. Ligands are shown using green sticks and atom-color spheres. Note the different conformation of the 'glutarate sensor' (Lys699 and Tyr700) in (B), which is caused by the absence of a glutarate moiety in the phosphate complex.

of the aspartyl residue of NAAG. This mechanism, which we derive from the structures described herein, is very similar to what has been observed for metalloproteinases such as thermolysin, and carboxypeptidases (Holz *et al*, 2003).

Substrate recognition

The inhibitor, GPI-18431, occupies the S1 and S1′ substrate-binding sites of GCPII (Figures 4 and 5), whereas the product of the cleavage reaction, L-glutamate, resides in the S1′ pocket only. The weak inhibitor, phosphate, only ligates the zinc ions in the active site. Both in the complexes with GPI-18431 and with glutamate, the C-terminal α-carboxylate group is recognized by Arg210 through a strong ion pair (2.70, 2.81 Å), and by hydrogen bonds from the hydroxyl groups of Tyr552 (3.11, 3.17 Å) and Tyr700 (2.48, 2.62 Å—in this paragraph, the first number refers to the GPI-18431 complex, the second to the glutamate complex). The glutarate portion of the bound GPI-18431 and L-glutamate bind in exactly the same way (Figure 4A and C). The glutamate side chain is recognized by a strong salt bridge (2.77, 2.58 Å) between the γ-carboxylate and Lys699 and also by a hydrogen bond (2.96, 3.00 Å) with the side-chain amide of Asn257 (Figures 4A, C and 5). The free amino group of the L-glutamate makes interactions with the γ-carboxylate of Glu424 (2.69 Å), with the carbonyl oxygen of Gly518 (2.90 Å), and with a water molecule that in turn is hydrogen-bonded to the phenolic hydroxyl group of Tyr552.

It is of interest that in the phosphate complex (Figure 4B), which has an unoccupied glutamate-binding (S1′) site, the loop carrying Lys699-Tyr700 adopts a conformation which is fairly flexible, as judged from the weak electron density, and very different from what is seen in the two structures harboring a glutarate group in the S1′ binding site. This is because of the missing interaction between Tyr700 OH and the α-carboxylate group of glutamate, as well as between Lys699 Nζ and the γ-carboxylate group of glutamate, as seen

©2006 European Molecular Biology Organization

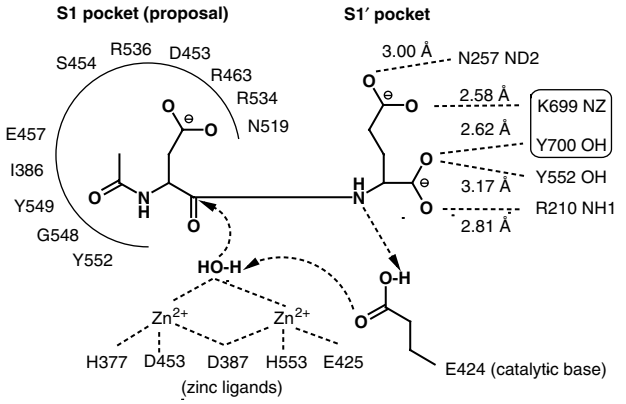

Figure 5 Scheme of the catalytic site, indicating the NAAG substrate as bound to the enzyme. The binding of the NAA portion of the substrate to the S1 pocket (left) is modeled, whereas the interactions of the glutamate residue to the S1′ pocket (right) are taken from the crystal structure of the glutamate complex (cf. Figure 4C). Residues Lys699 and Tyr700 of the 'glutarate sensor' are boxed. The first step in the catalytic reaction could be activation of the central nucleophile, HO–H, through the general base, Glu424. This is followed by the nucleophilic attack of the generated hydroxyl ion onto the peptidic bond of the substrate. After cleavage, Glu424 shuttles the proton to the amino group of the leaving product. Arrows run from nucleophile to electrophile.

in both the product and GPI-18431 inhibitor complexes (Figure 4A and C). In the complexes with an occupied glutamate-binding site, residues 692–704 form the β15/β16 hairpin (strand 692–695—turn—strand 699–704), whereas this is replaced by several consecutive, relatively mobile loops in the phosphate complex (and presumably in the free enzyme), with r.m.s.d. values of up to 7.6 Å for side-chain atoms between the two conformations. The hydroxyl group of Tyr700 itself exhibits a positional difference of 4.7 Å (Figure 3). Clearly, this is a strong indication for an induced-fit mechanism of substrate recognition by GCPII. Because of its obvious role in probing the S1′ pocket for the presence or absence of glutamate (or the glutarate portion of an inhibitor), we name the β15/β16 hairpin including the side chains of Lys699 and Tyr700 the 'glutarate sensor'.

The present structures also allow discussion of possible binding modes of the *N*-acetyl-aspartyl (NAA) portion of the NAAG substrate. The NAA very likely binds into a pocket (S1) lined with arginines 463, 534, and 536, as well as Ser454 and Asn519 (Figure 5). In all three structures described here, this binding site is filled by one or two water molecules because of the lack of a corresponding chemical moiety on the inhibitor. At the 'bottom' of the S1 pocket, there is a chloride ion (Figure 4) bound in a distorted octahedral manner to Arg534 (Nε, 3.36 Å, Nη2, 3.48 Å), Arg580 (Nη2, 3.92 Å), Asp453 main-chain NH (3.38 Å), Asn451 (Nδ2, 3.33 Å), and two water molecules (3.09 and 3.15 Å). The main task of the Cl^- is to hold Arg534 in an 'all-gauche' conformation, which is energetically not the most favorable. Presumably, Arg534 can interact with the aspartyl side chain of NAAG through its Nη1 and perhaps also Nη2 atom, while maintaining the coordination of the chloride. Interestingly, Robinson *et al* (1987) observed an absolute dependence of GCPII activity on monovalent anions, with chloride being the most efficient. From our structure, it is conceivable that in the absence of the chloride ion, Arg534 would adopt a conformation not allowing it to interact with the substrate.

The hydrophobic *p*-iodobenzyl (P1) group of GPI-18431 is oriented along the substrate-binding cleft (Figures 4A and 5). On one side, it interacts with the presumable specificity site for the aspartyl side chain of NAAG, making hydrogen bonds between the iodine and the guanidinium group of Arg536 (4.15 Å) as well as with the hydroxyl group of Ser454 (3.85 Å). On the other side, hydrophobic forces predominate, with interactions between the iodine and the phenyl ring of Tyr549 (approximately 3.8 Å), and an edge-to-face interaction between the aromatic rings of the inhibitor and Tyr552 (3.5 Å). The S1 binding site appears to be only partially filled by the inhibitor, and it is conceivable that much larger P1 moieties could be accommodated.

Discussion

Comparison with the transferrin receptor

The crystal structure of the extracellular portion of GCPII reveals that it consists of three domains, all of which are involved in substrate binding. This domain organization is very different from the prediction of six individual domains for GCPII by Rawlings and Barrett (1997). However, there is a pronounced similarity of the GCPII structure to the structure of the transferrin receptor (TfR) (Lawrence *et al*, 1999; Bennett *et al*, 2000), in spite of the latter not having any enzymatic activity (see Supplementary Table 3 for details). The sequence identity between the two proteins is 28%. The protease domain I has lost its catalytic center in the TfR and none of the zinc-binding ligands with the sole exception of Asp453 (GCPII numbering) are conserved. There are also many amino-acid replacements in the pocket that forms the substrate-binding site of GCPII. For example, the arginine residues very likely involved in NAAG recognition in GCPII (residues 463, 534, and 536 in the S1 pocket, and 210 in S1′) are not conserved in the TfR. In domain III, the two loops between helices α18 and α19 have a significantly different conformation in the TfR, with the second of them (corresponding to the β15/β16 hairpin—the 'glutarate sensor'—of GCPII) being much shorter and unable to reach into the domain I–II interface and into what is the substrate-binding site in GCPII.

Role of glycosylation

Glycosylation of GCPII has been shown to be essential for the catalytic activity of the enzyme (Ghosh and Heston, 2003; Barinka *et al*, 2004). We were able to identify seven out of the 10 sugar chains attached to asparagine residues in the recombinant ectodomain. The sugar residues linked to Asn638 (domain III, helix α17), which are clearly seen in the electron density map up to the forth sugar unit, Man_{II}, are involved in homodimer formation. Dimerization of the enzyme is essential for GCPII activity (Schulke *et al*, 2003); interestingly, the most dramatic loss of enzymatic activity in deglycosylation experiments was observed upon removal of the carbohydrate at Asn638 (Barinka *et al*, 2004). In the TfR, Asn638 is replaced by aspartate and therefore not glycosylated. Yet the TfR forms a similar homodimer; the lack of glycosylation at this position seems to be compensated for by the more extended TfR C-terminus that is involved in monomer–monomer contacts.

 ©2006 European Molecular Biology Organization

Role of the calcium ion

The Ca^{2+} binding site that we found in the GCPII structure is conserved in the TfR but in the aminopeptidase from *S. griseus* (SgAP; Greenblatt *et al*, 1997), it is located on the opposite site of the molecule. In SgAP, calcium ions enhance the thermal stability of the enzyme and modulate its activity and affinity towards substrates and inhibitors (Papir *et al*, 1998). In both the TfR and in GCPII, treatment with metal chelators leads to loss of biological activity (Orberger *et al*, 2001; Schulke *et al*, 2003). Our structure suggests that calcium binding helps stabilize the loop 272–279 that is involved in dimerization, a process essential for GCPII carboxypeptidase activity. Most interestingly, two of the sugar moieties attached to Asn638 make intermolecular contacts to the γ-carboxylate group of Glu276, thereby further stabilizing the loop 272–279. Similar to Ca^{2+} removal, deglycosylation at Asn638 will negatively influence the fold stability around residues 272–279.

Receptor-like properties of GCPII

Human GCPII has several features characteristic of receptor proteins, such as sequence signatures for endocytic internalization (Liu *et al*, 1998; Rapoport *et al*, 1998; Rajasekaran *et al*, 2003), or binding to filamin A, resulting in GCPII localization to the recycling endosomal compartment (Anilkumar *et al*, 2003). All of this raises the appealing possibility of GCPII functioning as a receptor for an as yet unidentified ligand. Interestingly, our crystal structure revealed the presence of a polyproline type-II helix on the surface of GCPII domain II. This structural motif usually mediates protein–protein interactions with Src homology 3 (SH3) domains. Even though SH3 domains are mainly restricted to the cell cytoplasm, recent evidence suggests the presence of SH3-like modules in extracellular proteins (Lougheed *et al*, 2001; Stoll *et al*, 2001). Taken together, apart from its hydrolytic function and likely involvement in folate transport across the membrane, GCPII might be implicated in other physiological processes such as transmembrane signalling or receptor–ligand interactions.

Processing of poly-γ-glutamates by GCPII

The glutamate in our crystal structure of the product complex, as well as the glutarate portion of GPI-18431 in the inhibitor complex of GCPII, are fully buried inside the protein, at the far end of the deep amphipathic funnel (Figure 3). One side of the funnel is formed by the aromatic rings of Tyr552 and Tyr700 (green in Figure 3), whereas the other side is paved with four arginine residues (463, 511, 534, and 536) that provide a positively charged patch (blue in Figure 3) guiding the poly-γ-glutamate to the catalytic site. Importantly, these arginine residues do not form the binding site for the C-terminal glutamate, which instead 'slips' into the deeply buried S1′ pocket where its α-carboxylate accepts three crucial hydrogen bonds from the side chains of Arg210, Tyr552, and Tyr700, whereas the γ-carboxy group interacts with the side chains of Asn257 and Lys699. How then can the glutamate products leave the substrate-binding site in case of the polymeric GCPII substrate, folyl-poly-γ-glutamate? It would be uneconomic for the enzyme to bind this substrate, release it along with the glutamate product after cleavage, and rebind it to cleave off the next glutamate residue. Interestingly, the structure of the phosphate complex, which has the S1′ pocket unoccupied, reveals the presence of a small hole at the 'backside' of the subsite (not shown). This is due to the withdrawal of the 'glutarate sensor', that is, the β15/β16 hairpin with Lys699 and Tyr700, from the S1′ pocket in this structure (which corresponds to the free enzyme). Assuming that the apical domain can move a bit with respect to the catalytic domain, it is very well possible that glutamate can leave the active site via this backdoor into the large space of the central cup formed by the conical shape of the dimer (Figure 2A). In this way, bound poly-γ-glutamates do not need to be released first in order to liberate the cleaved glutamate but instead, can translocate their chain by one position after each C-terminal cleavage step in order to place the new terminal glutamate into the S1′ pocket for hydrolysis. The concept of different access and egress sites for GCPII cleavage of the polymeric substrate is reminiscent of what has been proposed for the aminopeptidase dipeptidyl peptidase IV (Engel *et al*, 2003).

Prostate-specific membrane antigen

Recently, a crystal structure of ligand-free PSMA was published at a resolution of 3.5 Å (Davis *et al*, 2005). The overall fold of that model is similar to the one revealed here. Interestingly, the loop comprising residues Lys699 and Tyr700 (the 'glutarate sensor') is also withdrawn from the (empty) S1′ pocket in the structure of ligand-free PSMA, similarly to our structure of the phosphate complex. However, Davis *et al* (2005) did not locate the calcium and the chloride ions, both of which are essential for catalytic activity. Furthermore, they misinterpreted the features of the substrate-binding site by docking the NAAG substrate in the wrong orientation, with the *N*-acetyl-aspartyl portion of the ligand occupying the glutamate-binding site (S1′) and the glutamate moiety in the S1 pocket. The docking studies involving inhibitors such as 2-PMPA and a homology model of GCPII constructed on the basis of the TfR crystal structure (Rong *et al*, 2002) were equally wrong. This supports our view (Hillisch *et al*, 2004) that homology models and low-resolution X-ray structures can be useful in drug discovery to obtain a preliminary picture of a drug target but that only high-resolution crystal structures can provide the necessary detail for designing inhibitors.

Design of new GCPII inhibitors

The structures presented here help in both understanding the observed structure–activity relationships as well as the design of new inhibitors. Two major classes of inhibitors have been reported, one featuring a phosphinate moiety (Jackson *et al*, 1996) and the other bearing a thiol (Majer *et al*, 2003), as a zinc ligand. The importance of the pentanedioic acid (glutarate) moiety as a glutamate mimic in the P1′ position for inhibitor potency is well established in both series. In general, we observed much stricter structural requirements (e.g. in terms of side-chain length) in the phosphinate series compared to their thiol counterparts. This could be due to the more rigid bidentate nature of the phosphinate–catalytic zinc interaction compared to the more flexible monodentate coordination of a thiol group.

For the P1 position of the inhibitors, the structure–activity relationships are consistent with our structural findings, that is, there are few hydrophobic residues available in the S1 pocket and the P1 group only makes hydrophobic

©2006 European Molecular Biology Organization

interactions with the side chains of Tyr549 and Tyr552. Introduction of any substituent to the inhibitor nonprime area led to a decrease of potency, with the marked exception of carboxylate-containing groups (Slusher *et al*, 1990). The additional carboxylate likely mimics, in part, the NAA portion of the natural substrate.

Conclusions

Crystallographic analysis of GCPII revealed a three-domain organization of the monomer. Dimer formation relies not only on interactions between amino-acid side chains, but also involves the carbohydrate chain attached to Asn638. The three crystal structures of GCPII presented here correspond to different states of the substrate-binding site. In the complex with the inhibitor, GPI-18431, the S1′ pocket is filled by the glutarate portion of the compound, and the S1 site is partly occupied by the iodo-benzyl moiety. In the complex with the product of the reaction, L-glutamate, the active site is unligated and most likely seen in the state that it adopts in the free enzyme. In the phosphate complex, the substrate-specificity sites S1 and S1′ remain unoccupied; interestingly, in this structure, the 'glutarate sensor' (the β15/β16 hairpin), which is involved in glutarate recognition in S1′, retracts itself, indicating that substrate recognition by GCPII involves an induced-fit mechanism. With this high-resolution structure at hand, it will now be possible to design improved inhibitors of GCPII.

Materials and methods

The recombinant form of human GCPII, amino-acid residues 44–750 (ectodomain), was prepared as described by Barinka *et al* (2002), employing heterologous expression in stable transfected Schneider cells. For growing crystals at room temperature, hanging drops were assembled by mixing 2 μl protein solution with 2 μl well solution. Wells contained 20 mM HEPES pH 7.25, 200 mM NaCl, 5% (w/v) PEG 400, and 15% (w/v) PEG 1500. Especially in the presence of GPI-18431 (2 mM in protein solution), large crystals of up to $0.6 \times 0.25 \times 0.2\,mm^3$ grew within 1–2 weeks. The crystals turned out to be very radiation-sensitive and in addition could not be reproducibly flash-cooled. However, from crystals mounted in short capillaries, full diffraction data sets were easily obtained at 263 K at the Deutsches-Elektronen Synchrotron (DESY), EMBL beam lines X13 and BW7A. The two bound zinc ions in the active site did not provide sufficient phase information but allowed to discriminate between space groups I222 (correct) and $I2_12_12_1$ (false), with cell dimensions $a = 103.13$, $b = 131.19$, $c = 161.23$ Å, and one molecule of GCPII in the asymmetric unit. In order to obtain usable phase information, the iodinated inhibitor (*S*)-2-(4-iodobenzylphosphonomethyl)-pentanedioic acid (GPI-18431) was synthesized (Tsukamoto *et al*, 2005) and cocrystallized with the enzyme. The 2.0-Å resolution data were collected at BW7A at a wavelength of 1.26 Å, that is, near the zinc absorption maximum, at which iodine also gives a strong anomalous signal. Good starting phases were calculated with a SAD protocol in SOLVE (Terwilliger, 2002), revealing three heavy-atom positions, one of which was the iodine. A good starting model was obtained with ARP/wARP (Morris *et al*, 2002). The model was further refined and completed running Refmac5 (Murshudov, 1997) and Xtalview (McRee, 1999). Other programs used were from the CCP4 suite (Collaborative Computational Project No. 4, 1994). For structural comparisons, ALIGN (Cohen, 1997) and the DALI server (http://www.ebi.ac.uk/dali/; Holm and Sander, 1998) were used.

Supplementary data

Supplementary data are available at *The EMBO Journal* Online.

Acknowledgements

The contribution of Karen Henning to the early crystallization experiments with GCPII is acknowledged. JRM thanks Dr Boaz Shaanan of the Ben Gurion University, Israel, for providing the Linux code of the program ALIGN. CB was supported by a short-term fellowship from FEBS. JK acknowledges support from the Grant Agency of the Czech Republic, Grant 301/03/0784, and from MSMT CR, Grant 1M6138896301. RH thanks the Fonds der Chemischen Industrie for continuous support.

Accession Numbers

Atomic coordinates of the structures described here as well as the experimental diffraction amplitudes have been deposited at the RCSB Protein Data Bank with accession numbers 2C6C (complex with GPI-18431), 2C6P (phosphate complex), and 2C6G (glutamate complex).

References

Anilkumar G, Rajasekaran SA, Wang S, Hankinson O, Bander NH, Rajasekaran AK (2003) Prostate-specific membrane antigen association with filamin A modulates its internalization and NAALADase activity. *Cancer Res* **63:** 2645–2648

Barinka C, Rinnova M, Sacha P, Rojas C, Majer P, Slusher BS, Konvalinka J (2002) Substrate specificity, inhibition and enzymological analysis of recombinant human glutamate carboxypeptidase II. *J Neurochem* **80:** 477–487

Barinka C, Sacha P, Sklenar J, Man P, Bezouska K, Slusher BS, Konvalinka J (2004) Identification of the *N*-glycosylation sites on glutamate carboxypeptidase II necessary for proteolytic activity. *Protein Sci* **13:** 1627–1635

Bennett MJ, Lebron JA, Bjorkman PJ (2000) Crystal structure of the hereditary haemochromatosis protein HFE complexed with transferrin receptor. *Nature* **403:** 46–53

Benveniste H, Drejer J, Schousboe A, Diemer NH (1984) Elevation of the extracellular concentrations of glutamate and aspartate in rat hippocampus during transient cerebral ischemia monitored by intracerebral microdialysis. *J Neurochem* **43:** 1369–1374

Berger UV, Carter RE, Coyle JT (1995) The immunocytochemical localization of *N*-acetylaspartyl glutamate, its hydrolysing enzyme NAALADase, and the NMDAR-1 receptor at a vertebrate neuromuscular junction. *Neuroscience* **64:** 847–850

Bruno V, Battaglia G, Copani A, Giffard RG, Raciti G, Raffaele R, Shinozaki H, Nicoletti F (1995) Activation of class II or III metabotropic glutamate receptors protects cultured cortical neurons against excitotoxic degeneration. *Eur J Neurosci* **7:** 1906–1913

Butcher SP, Bullock R, Graham DI, McCulloch J (1990) Correlation between amino acid release and neuropathologic outcome in rat brain following middle cerebral artery occlusion. *Stroke* **21:** 1727–1733

Carpenter KJ, Sen S, Matthews EA, Flatters SL, Wozniak KM, Slusher BS, Dickenson AH (2003) Effects of GCP-II inhibition on responses of dorsal horn neurones after inflammation and neuropathy: an electrophysiological study in the rat. *Neuropeptides* **37:** 298–306

Carter RE, Feldman AR, Coyle JT (1996) Prostate-specific membrane antigen is a hydrolase with substrate and pharmacologic characteristics of a neuropeptidase. *Proc Natl Acad Sci USA* **93:** 749–753

Chen SR, Wozniak KM, Slusher BS, Pan HL (2002) Effect of 2-(phosphono-methyl)-pentanedioic acid on allodynia and afferent ectopic discharges in a rat model of neuropathic pain. *J Pharmacol Exp Ther* **300:** 662–667

Chevrier B, Schalk C, D'Orchymont H, Rondeau JM, Moras D, Tarnus C (1994) Crystal structure of *Aeromonas proteolytica*

 ©2006 European Molecular Biology Organization

aminopeptidase: a prototypical member of the co-catalytic zinc enzyme family. *Structure* **2:** 283–291

Cohen GE (1997) ALIGN: a program to superimpose protein coordinates, accounting for insertions and deletions. *J Appl Crystallogr* **30:** 1160–1161

Collaborative Computational Project No. 4 (1994) The CCP4 suite: programs for protein crystallography. *Acta Crystallogr D* **50:** 760–763

Coyle JT (1997) The nagging question of the function of *N*-acetyl-aspartylglutamate. *Neurobiol Dis* **4:** 231–238

Davis MI, Bennett MG, Thomas LM, Bjorkman PJ (2005) Crystal structure of prostate-specific membrane antigen, a tumor marker and peptidase. *Proc Natl Acad Sci USA* **102:** 5981–5986

Doble A (1999) The role of excitotoxicity in neurodegenerative disease: implications for therapy. *Pharmacol Ther* **81:** 163–221

Engel M, Hoffmann T, Wagner L Wermann M, Heiser U, Kiefersauer R, Huber R, Bode W, Demuth H-U, Brandstetter H (2003) The crystal structure of dipeptidyl peptidase IV (CD26) reveals its functional regulation and enzymatic mechanism. *Proc Natl Acad Sci USA* **100:** 5063–5068

Fagg GE, Foster AC, Ganong AH (1986) Excitatory amino acid synaptic mechanisms and neurological function. *Trends Pharmacol Sci* **7:** 357–363

Ghadge GD, Slusher BS, Bodner A, Canto MD, Wozniak K, Thomas AG, Rojas C, Tsukamoto T, Majer P, Miller RJ, Monti AL, Roos RP (2003) Glutamate carboxypeptidase II inhibition protects motor neurons from death in familial amyotrophic lateral sclerosis models. *Proc Natl Acad Sci USA* **100:** 9554–9559

Ghosh A, Heston WD (2003) Effect of carbohydrate moieties on the folate hydrolysis activity of the prostate specific membrane antigen. *Prostate* **57:** 140–151

Ghosh A, Heston WD (2004) Tumor target prostate specific membrane antigen (PSMA) and its regulation in prostate cancer. *J Cell Biochem* **91:** 528–539

Greenblatt HM, Almog O, Maras B, Spungin-Bialik A, Barra D, Blumberg S, Shoham G (1997) Streptomyces griseus aminopeptidase: X-ray crystallographic structure at 1.75 Å resolution. *J Mol Biol* **265:** 620–636

Heston WD (1997) Characterization and glutamyl preferring carboxypeptidase function of prostate specific membrane antigen: a novel folate hydrolase. *Urology* **49:** 104–112

Hillisch A, Pineda LF, Hilgenfeld R (2004) Utility of homology models in the drug discovery process. *Drug Discov Today* **9:** 659–669

Holm L, Sander C (1998) Dictionary of recurrent domains in protein structures. *Proteins* **33:** 88–96

Holmes EH, Greene TG, Tino WT, Boynton AL, Aldape HC, Misrock SL, Murphy GP (1996) Analysis of glycosylation of prostate-specific membrane antigen derived from LNCaP cells, prostatic carcinoma tumors, and serum from prostate cancer patients. *Prostate Suppl* **7:** 25–29

Holz RC, Bzymek KP, Swierczek SI (2003) Co-catalytic metallopeptidases as pharmaceutical targets. *Curr Opin Chem Biol* **7:** 197–206

Jackson PF, Cole DC, Slusher BS, Stetz SL, Ross LE, Donzanti BA, Trainor DA (1996) Design, synthesis, and biological activity of a potent inhibitor of the neuropeptidase *N*-acetylated alpha-linked acidic dipeptidase. *J Med Chem* **39:** 619–622

Jackson PF, Slusher BS (2001) Design of NAALADase inhibitors: a novel neuroprotective strategy. *Curr Med Chem* **8:** 949–957

Jackson PF, Tays KL, Maclin KM, Ko YS, Li W, Vitharana D, Tsukamoto T, Stoermer D, Lu XC, Wozniak K, Slusher BS (2001) Design and pharmacological activity of phosphinic acid based NAALADase inhibitors. *J Med Chem* **44:** 4170–4175

Kozikowski AP, Zhang J, Nan F, Petukhov PA, Grajkowska E, Wroblewski JT, Yamamoto T, Bzdega T, Wroblewska B, Neale JH (2004) Synthesis of urea-based inhibitors as active site probes of glutamate carboxypeptidase II: efficacy as analgesic agents. *J Med Chem* **47:** 1729–1738

Lawrence CM, Ray S, Babyonyshev M, Galluser R, Borhani DW, Harrison SC (1999) Crystal structure of the ectodomain of human transferrin receptor. *Science* **286:** 779–782

Liu H, Rajasekaran AK, Moy P, Xia Y, Kim S, Navarro V, Rahmati R, Bander NH (1998) Constitutive and antibody-induced internalization of prostate-specific membrane antigen. *Cancer Res* **58:** 4055–4060

Lougheed JC, Holton JM, Alber T, Bazan JF, Handel TM (2001) Structure of melanoma inhibitory activity protein, a member of a recently identified family of secreted proteins. *Proc Natl Acad Sci USA* **98:** 5515–5520

Majer P, Jackson PF, Delahanty G, Grella BS, Ko YS, Li W, Liu Q, Maclin KM, Polakova J, Shaffer KA, Stoermer D, Vitharana D, Wang EY, Zakrzewski A, Rojas C, Slusher BS, Wozniak KM, Burak E, Limsakun T, Tsukamoto T (2003) Synthesis and biological evaluation of thiol-based inhibitors of glutamate carboxypeptidase II: discovery of an orally active GCP II inhibitor. *J Med Chem* **46:** 1989–1996

McRee DE (1999) XtalView/Xfit—A versatile program for manipulating atomic coordinates and electron density. *J Struct Biol* **125:** 156–165

Morris RJ, Perrakis A, Lamzin VS (2002) ARP/wARP's model-building algorithms I. The main chain. *Acta Crystallogr D* **58:** 968–975

Murshudov GN (1997) Refinement of macromolecular structures by the maximum-likelihood method. *Acta Crystallogr D* **53:** 240–255

Orberger G, Fuchs H, Geyer R, Gessner R, Kottgen E, Tauber R (2001) Structural and functional stability of the mature transferrin receptor from human placenta. *Arch Biochem Biophys* **386:** 79–88

Papir G, Spungin-Bialik A, Ben-Meir D, Fudim E, Gilboa R, Greenblatt HM, Shoham G, Lessel U, Schomburg D, Ashkenazi R, Blumberg S (1998) Inhibition of *Streptomyces griseus* aminopeptidase and effects of calcium ions on catalysis and binding—comparisons with the homologous enzyme *Aeromonas proteolytica* aminopeptidase. *Eur J Biochem* **258:** 313–319

Pinto JT, Suffoletto BP, Berzin TM, Qiao CH, Lin S, Tong WP, May F, Mukherjee B, Heston WD (1996) Prostate-specific membrane antigen: a novel folate hydrolase in human prostatic carcinoma cells. *Clin Cancer Res* **2:** 1445–1451

Puttfarcken PS, Handen JS, Montgomery DT, Coyle JT, Werling LL (1993) *N*-acetyl-aspartylglutamate modulation of *N*-methyl-D-aspartate-stimulated [^{3}H]norepinephrine release from rat hippocampal slices. *J Pharmacol Exp Ther* **266:** 796–803

Rajasekaran SA, Anilkumar G, Oshima E, Bowie JU, Liu H, Heston W, Bander NH, Rajasekaran AK (2003) A novel cytoplasmic tail MXXXL motif mediates the internalization of prostate-specific membrane antigen. *Mol Biol Cell* **14:** 4835–4845

Rapoport I, Chen YC, Cupers P, Shoelson SE, Kirchhausen T (1998) Dileucine-based sorting signals bind to the beta chain of AP-1 at a site distinct and regulated differently from the tyrosine-based motif-binding site. *EMBO J* **17:** 2148–2155

Rawlings ND, Barrett AJ (1997) Structure of membrane glutamate carboxypeptidase. *Biochim Biophys Acta* **1339:** 247–252

Rawlings ND, Tolle DP, Barrett AJ (2004) *MEROPS*: the peptidase database. *Nucleic Acids Res* **32:** D160–D164

Robinson MB, Blakely RD, Couto R, Coyle JT (1987) Hydrolysis of the brain dipeptide *N*-acetyl-L-aspartyl-L-glutamate Identification and characterization of a novel *N*-acetylated alpha-linked acidic dipeptidase activity from rat brain. *J Biol Chem* **262:** 14498–14506

Rogawski MA (1993) Therapeutic potential of excitatory amino acid antagonists: channel blockers and 2,3-benzodiazepines. *Trends Pharmacol Sci* **14:** 325–331

Rong SB, Zhang J, Neale JH, Wroblewski JT, Wang S, Kozikowski AP (2002) Molecular modeling of the interactions of glutamate carboxypeptidase II with its potent NAAG-based inhibitors. *J Med Chem* **45:** 4140–4152

Schulke N, Varlamova OA, Donovan GP, Ma D, Gardner JP, Morrissey DM, Arrigale RR, Zhan C, Chodera AJ, Surowitz KG, Maddon PJ, Heston WD, Olson WC (2003) The homodimer of prostate-specific membrane antigen is a functional target for cancer therapy. *Proc Natl Acad Sci USA* **100:** 12590–12595

Sekiguchi M, Okamoto K, Sakai Y (1989) Low-concentration *N*-acetylaspartyl-glutamate suppresses the climbing fiber response of Purkinje cells in guinea pig cerebellar slices and the responses to excitatory amino acids of *Xenopus laevis* oocytes injected with cerebellar mRNA. *Brain Res* **482:** 87–96

Shaw PJ, Ince PG (1997) Glutamate, excitotoxicity and amyotrophic lateral sclerosis. *J Neurol* **244** (Suppl 2)**:** S3–S14

Slusher BS, Robinson MB, Tsai G, Simmons ML, Richards SS, Coyle JT (1990) Rat brain *N*-acetylated alpha-linked acidic dipeptidase activity. Purification and immunologic characterization. *J Biol Chem* **265:** 21297–21301

Slusher BS, Vornov JJ, Thomas AG, Hurn PD, Harukuni I, Bhardwaj A, Traystman RJ, Robinson MB, Britton P, Lu XC, Tortella FC,

©2006 European Molecular Biology Organization

Wozniak KM, Yudkoff M, Potter BM, Jackson PF (1999) Selective inhibition of NAALADase, which converts NAAG to glutamate, reduces ischemic brain injury. *Nat Med* **5:** 1396–1402

Speno HS, Luthi-Carter R, Macias WL, Valentine SL, Joshi AR, Coyle JT (1999) Site-directed mutagenesis of predicted active site residues in glutamate carboxypeptidase II. *Mol Pharmacol* **55:** 179–185

Stoll R, Renner C, Zweckstetter M, Bruggert M, Ambrosius D, Palme S, Engh RA, Golob M, Breibach I, Buettner R, Voelter W, Holak TA, Bosserhoff AK (2001) The extracellular human melanoma inhibitory activity (MIA) protein adopts an SH3 domain-like fold. *EMBO J* **20:** 340–349

Su SL, Huang IP, Fair WR, Powell CT, Heston WD (1995) Alternatively spliced variants of prostate-specific membrane antigen RNA: ratio of expression as a potential measurement of progression. *Cancer Res* **55:** 1441–1443

Tasch J, Gong M, Sadelain M, Heston WD (2001) A unique folate hydrolase, prostate-specific membrane antigen (PSMA): a target for immunotherapy? *Crit Rev Immunol* **21:** 249–261

Terwilliger TC (2002) Automated structure solution, density modification and model building. *Acta Crystallogr D* **58:** 1937–1940

Tiffany CW, Lapidus RG, Merion A, Calvin DC, Slusher BS (1999) Characterization of the enzymatic activity of PSM: comparison with brain NAALADase. *Prostate* **39:** 28–35

Tsukamoto T, Majer P, Vitharana D, Ni C, Hin B, Lu X-CM, Thomas AG, Wozniak KM, Calvin DC, Wu Y, Slusher BS, Scarpetti D, Bonneville GW (2005) Enantiospecificity of glutamate carboxypeptidase II inhibition. *J Med Chem* **48:** 2319–2324

Urazaev AK, Buttram Jr JG, Deen JP, Gafurov BS, Slusher BS, Grossfeld RM, Lieberman EM (2001) Mechanisms for clearance of released *N*-acetylaspartylglutamate in crayfish nerve fibers: implications for axon-glia signaling. *Neuroscience* **107:** 697–703

Wroblewska B, Wroblewski JT, Pshenichkin S, Surin A, Sullivan SE, Neale JH (1997) *N*-acetylaspartylglutamate selectively activates mGluR3 receptors in transfected cells. *J Neurochem* **69:** 174–181

Yamamoto T, Nozaki-Taguchi N, Sakashita Y (2001a) Spinal *N*-acetyl-alpha-linked acidic dipeptidase (NAALADase) inhibition attenuates mechanical allodynia induced by paw carrageenan injection in the rat. *Brain Res* **909:** 138–144

Yamamoto T, Nozaki-Taguchi N, Sakashita Y, Inagaki T (2001b) Inhibition of spinal *N*-acetylated-alpha-linked acidic dipeptidase produces an antinociceptive effect in the rat formalin test. *Neuroscience* **102:** 473–479

Zhang W, Slusher B, Murakawa Y, Wozniak KM, Tsukamoto T, Jackson PF, Sima AA (2002) GCPII (NAALADase) inhibition prevents long-term diabetic neuropathy in type 1 diabetic BB/Wor rats. *J Neurol Sci* **194:** 21–28

©2006 European Molecular Biology Organization